HHS Public Access

Author manuscript

J Cell Biochem. Author manuscript; available in PMC 2021 April 01.

Published in final edited form as:

J Cell Biochem. 2020 April ; 121(4): 2909–2926. doi:10.1002/jcb.29532.

Mediator Subunit MED1 Modulates Intranuclear Dynamics of the Thyroid Hormone Receptor

Matthew R. Femia, **Rochelle M. Evans**, **Jibo Zhang**, **Xiaopeng Sun**, **Caroline J. Lebegue**, **Vincent R. Roggero**, **Lizabeth A. Allison**

Department of Biology, College of William and Mary, Williamsburg, VA, 23185, U.S.A.

Abstract

The thyroid hormone receptors (TRs) mediate thyroid hormone (T_3)-dependent gene expression. The nuclear import and export signals that direct TR shuttling are well characterized, but little is known about factors modulating nuclear retention. We used fluorescence-based nucleocytoplasmic scoring and fluorescence recovery after photobleaching (FRAP) in transfected cells to investigate whether Mediator subunits MED1 and MED13 play a role in nuclear retention of TR. When MED1 was overexpressed, there was a striking shift towards a greater nuclear localization of TRβ1 and the oncoprotein v-ErbA, subtypes with cytosolic populations at steady-state, and TRβ1 intranuclear mobility was reduced. For TRα1, there was no observable change in its predominantly-nuclear distribution pattern or mobility. Consistent with a role for MED1 in nuclear retention, the cytosolic TRα1 and TRβ1 population was significantly greater in MED1$^{-/-}$ cells, compared with MED1$^{+/+}$ cells. Exposure to T_3 and epidermal growth factor, which induces MED1 phosphorylation, also altered TR intranuclear dynamics. Overexpression of miR-208a, which downregulates MED13, led to a more cytosolic distribution of nuclear-localized TRα1; however, overexpression of MED13 had no effect on TRβ1 localization. The known binding site of MED1 overlaps with a transactivation domain and nuclear export signal in helix 12 of TR's ligand-binding domain (LBD). Coimmunoprecipitation assays demonstrated that TR's LBD interacts directly with exportins 5 and 7, suggesting that binding of exportins and MED1 to TR may be mutually exclusive. Collectively, our data provide evidence that MED1 promotes nuclear retention of TR, and highlight the dual functionality of helix 12 in TR transactivation and nuclear export.

Keywords

Thyroid hormone receptor; Mediator subunit 1 (MED1); Mediator subunit 13 (MED13); fluorescence recovery after photobleaching (FRAP); intranuclear mobility

1 INTRODUCTION

Thyroid hormone action is mediated primarily by two major subtypes of the thyroid hormone receptor, TRα1 and TRβ1, that are members of the nuclear receptor superfamily.

Correspondence: Lizabeth A. Allison, Department of Biology, College of William and Mary, 540 Landrum Drive, ISC 3030, Williamsburg, VA, 23185, U.S.A. laalli@wm.edu.

CONFLICTS OF INTEREST

The authors declare that there are no conflicts of interest.

By modulating the transcription of target genes in response to thyroid hormone (T_3), TR plays a key role in human health via the regulation of many aspects of development, growth, and metabolism, including energy homeostasis in the heart (1–10). TR function involves a multifaceted cascade of events that results in binding of TR, often as a heterodimer with the retinoid X receptor (RXR), to thyroid hormone response element (TREs), and culminates in the modulation of target gene expression (11–13). In the absence of ligand, TR binds positive TREs through two zinc fingers in the DNA-binding domain, and represses gene expression in conjunction with corepressors (14,15). Upon ligand binding, TR undergoes a conformational change, releasing corepressors and forming a docking surface for transcriptional coactivators in its activation domain (16–20). In addition to activating transcription, TRs can also repress gene expression in a T_3-dependent manner by binding to negative TREs (21–23).

Transcription factors, such as TRα1 and TRβ1, cross the nuclear envelope through the nuclear pore complexes, facilitated by transport proteins called importins and exportins (24–30). Although localized primarily to the nucleus at steady state, TRα1 and TRβ1 shuttle between the nucleus and cytosol, directed by multiple nuclear export signal (NES) and nuclear localization signal (NLS) motifs (31–34) (Fig. 1A). Along with a NLS in the hinge domain (NLS-1), TRα1 houses a NLS in the A/B domain that is absent in TRβ1 and inactive in the retroviral oncoprotein v-ErbA (31). v-ErbA is a dominant negative mutant of TRα1 that displays altered transport activity due to acquisition of a viral CRM1 (exportin 1)-dependent NES and localizes to both the nucleus and cytosol at steady state (35–38). TRα1 exits the nucleus through two pathways, one dependent on the export factors CRM1 and calreticulin, and the other CRM1-independent (39), mediated by NESs in helix H3 (NES-H3), helix H6 (NES-H6), and helix 12 (NES-H12) of the ligand-binding domain (LBD) of TR (31). Given that TR contains multiple, conflicting nuclear import and export signals, it is of interest to ascertain what factors modulate TR nuclear retention. Little is known regarding how TR intranuclear mobility and localization is regulated in the nucleus. Advances in live-cell imaging of other transcription factors, however, suggest that intrinsically disordered regions within transcription factor activation domains interact to form highly dynamic, high-concentration “hubs” that stabilize DNA binding, recruit RNA polymerase II, and activate transcription (40).

Here, we begin to tease apart the relative importance of coregulatory factors in TR localization, focusing on Mediator, an evolutionarily conserved multi-subunit complex that functionally bridges DNA-bound nuclear receptors and other signal-activated transcription factors with the general transcription apparatus (41–46). Mediator has emerged as an important player in many disorders, such as cancer, and cardiovascular, metabolic, and neurological diseases (43). TRα1 and TRβ1 directly bind with Mediator complex subunit 1 (MED1), originally called TRAP220 (Thyroid hormone receptor-associated protein 220) (47). Receptor binding domains present in MED1 contain leucine-rich (LXXLL) motifs which interact with the activation function 2 (AF-2) region of TR’s LBD in helix 12 (48–51) to facilitate transcription of T_3-responsive genes (52–55) (Fig. 1B). In addition, phosphorylation of MED1 by the mitogen-activated protein kinase (MAPK)-extracellular signal-regulated kinase (ERK) at specific threonine residues promotes its association with Mediator, and phosphorylated MED1 is a more potent coactivator of TR-regulated genes

(52,53). Adding to the complexity of TR regulatory networks, miR-208a, a cardiac-specific microRNA is upregulated in response to elevated T_3 levels (56–58). Among the targets of miR-208a is MED13, which associates with MED12 and cyclin C-cyclin dependent kinase 8 (CDK8) in a complex that is reversibly associated with Mediator (41,59,60). Components of the MED12/MED13/CDK8 module control the expression of a subset of genes, either through repression or activation (60–63). In the heart, MED13 suppresses TRβ1 transcriptional activation (60), but other data suggest that the MED12/MED13/CDK8 module can also play an important coactivator role in T_3-dependent transcription (64).

Given their importance in transcriptional regulation, we thus hypothesized that Mediator subunits MED1 and MED13 play a pivotal role in anchoring TR in the nucleus. In the current study, we demonstrate that MED1, and to a lesser extent MED13, promote nuclear retention of TR by altering intranuclear dynamics, underscoring how the dual functionality of helix 12 in TR's LBD serves to modulate both gene transactivation and nuclear export.

2 MATERIALS AND METHODS

2.1 Plasmids

mCherry-tagged TRα1, TRβ1, and v-ErbA expression plasmids were prepared by subcloning the corresponding coding regions from GFP-TRα1, GFP-v-ErbA (37) and GFP-TRβ1 (34) into pmCherry-C1 (Clontech). GFP-GST-GFP-Hinge, containing NLS-1 of TRα1, and GFP-GST-GFP-Hinge-LBD were previously described (31). GFPSpark-MED1 (Sino Biological Inc.) encodes a truncated human MED1 (residues 547–1581) that lacks the TR interaction domain. GFP-MED1 (OriGene Technologies, Inc.) encodes full-length human MED1 (residues 1–1581). The pEGFP-GR expression plasmid was a gift from Alice Wong (Addgene plasmid #47504). pCMV-MIR, a scrambled miRNA and GFP expression plasmid; and pCMV-MIR208a, a miR-208a and GFP expression plasmid, were from Origene Technologies, Inc. The expression plasmid for GFP-MED13, pEZ-M29-MED13, was obtained from GeneCopoeia™.

2.2 Cell culture and transfection

HeLa cells (ATCC #CCL-2) were cultured in Minimum Essential Medium (MEM, Gibco) supplemented with 10% fetal bovine serum (Gibco). $MED1^{+/+}$ ($Trap220^{+/+}$) and $MED1^{-/-}$ ($Trap220^{-/-}$) mouse embryonic fibroblasts (MEFs) were a generous gift from Dr. Robert Roeder, Rockefeller University (54). MEFs were cultured in Dulbecco's Modified Eagle Medium (DMEM, Gibco) supplemented with 10% newborn calf serum (Gibco). Six-well culture dishes were seeded at a density of 2.5×10^5 cells per well on round coverslips and transfected using Lipofectamine 2000 (Invitrogen) for HeLa cells, as described (65), and Lipofectamine 3000 for MEFs, according to the manufacturer's protocol. For hormone treatments, 8 h post-transfection, transfection mixtures were replaced with 10% charcoal-stripped FBS (Gibco) containing MEM, supplemented with 100 ng/ml recombinant human EGF (Gibco) (53), or 100 nM T_3 (MilliporeSigma) (37).

2.3 Analysis of nucleocytoplasmic distribution

Approximately 24–26 h post-transfection, cells were fixed in 3.7% formaldehyde (37), and coverslips were mounted in Fluoro-Gel II containing DAPI (Electron Microscopy Sciences) onto glass slides. Fluorescent fusion protein distribution was analyzed with a Nikon Plan Apo 40x/0.95 objective on a Nikon ECLIPSE TE 2000-E fluorescence microscope using the following filter sets: Nikon Ultraviolet Excitation via UV-2E/C filter for DAPI/nuclei visualization; Blue Excitation via B-2E/C filter block for GFP/FITC visualization; and Red Excitation via T-2E/C filter for mCherry/TRITC. A CoolSNAP HQ2 CCD camera (Photometrics) allowed image capture and NIS-Elements AR software (Nikon) was used for analysis. Slides were blinded by members of the lab to ensure scoring was performed without knowledge of treatment. A region of interest (ROI) was positioned inside both the nucleus and cytoplasm of cells and fluorescence intensity was recorded for each, with a minimum of three biological replicates and 100 ROI-analyzed cells per replicate. Nuclear to cytoplasmic (N/C) ratios were calculated and normalized to baseline conditions for corresponding biological replicates. A ratio greater than 1.0 was interpreted as having a more nuclear distribution, while less than 1.0 indicated a greater distribution of TR in the cytoplasm.

2.4 Fluorescence recovery after photobleaching (FRAP)

Approximately 24–29 h post-transfection, cells were washed with Dulbecco's phosphate buffered saline (D-PBS), then incubated in MEM-α in an OkoLab Incubation System (Warner Instruments, Inc.) at 37°C and 5% CO_2. To sequester v-ErbA in the nucleus, cells expressing mCherry-v-ErbA were supplemented with 5 ng/mL leptomycin B (MilliporeSigma), 45 min prior to analysis. To induce nuclear translocation of GFP-GR, cells were treated with 1 μM dexamethasone (MilliporeSigma) for 30 min prior to analysis. Strip-FRAP (66,67) was performed on a Nikon A1Rsi confocal microscope Ti-E-PFS (Nikon Inc.) with a 60x oil objective and perfect focus system, using the following laser lines: 488-nm line of krypton-argon laser for GFP, 561-nm line for mCherry detection, and solid-state 405-nm line for photobleaching. Acquisition and photobleaching were coordinated within NIS-Elements AR (Nikon). Using the stimulation module of NIS-Elements, the total experimental time for the assay was ~35 sec, with a frame rate of ~15 images per sec. After a 5 sec "pre-bleach" acquisition phase at ~2–3% laser power, the stimulation line ROI was positioned within a nucleus with relatively symmetrical morphology and subject to 1 sec of photobleaching at 100% laser power, followed by a post-bleach acquisition phase at 2–3% laser power. All image acquisition was conducted through resonant scanning, corrected by line averaging. Data from three separate, biologically independent replicates of 20 nuclei per replicate were analyzed.

FRAP data were normalized using standard methods (68). Equation 1 shows full normalization of fluorescence, I_{full}, as a function of time, where $I_{double\ norm}$ represents the background-corrected, double normalization of fluorescence and $t_{postbleach}$ is the background-corrected value at the time point immediately after bleaching has terminated. Effectively, the data were normalized from 0 – 1, where 0 was the lowest relative intensity, directly after the bleaching phase, and 1 was the point of greatest post-bleach recovery.

$$I(t)_{full} = \frac{I(t)_{double\,norm} - I\left(t_{postbleach}\right)_{double\,norm}}{1 - I\left(t_{postbleach}\right)_{double\,norm}} \quad (1)$$

Normalized data were then used to calculate the rate of recovery for each treatment. The recovery rate, post-bleach fluorescence recovery over time to equilibrium, was used as the primary measurement to evaluate changes in mobility. The normalized data were also used to estimate a half-time/$T_{1/2}$ value, or the time required for half of the total fluorescence to recover back into the bleached region. As our data were normalized to 1, we recorded the half-time as the time that elapsed between the end of the bleaching phase and the point at which 50% recovery occurred directly on the full-normalized recovery curve. The mobile fraction was calculated using Equation 2

$$F_m = \frac{I\left(t_{eq}\right) - I\left(t_{postbleach}\right)}{I\left(t_{pre}\right) - I\left(t_{postbleach}\right)} \quad (2)$$

where F_m, is the mobile fraction, $I(t_{eq})$ is the full normalized intensity at which recovery equilibrium is reached, $I(t_{pre})$ is defined by the intensity pre-bleach, and $I(t_{postbleach})$ is the intensity at time (t), directly after bleaching. Subsequently, the immobile fraction F_i was calculated using Equation 3

$$F_i = 1 - F_m \quad (3)$$

2.5 Statistical analysis

All data are expressed as mean ± SEM. All *p*-values were two-tailed, and $p \leq 0.05$ was considered statistically significant.

2.6 GFP-Trap® coimmunoprecipitation

HeLa cells were seeded on 100 mm vented plates at a concentration of 9×10^5 cells per plate in MEM supplemented with 10% FBS. Twenty-four hours post-seeding, each plate was transfected with expression plasmids encoding GFP, GFP-TRα1 or GFP-GST-GFP-Hinge-LBD, using Lipofectamine 2000. After 26 h, GFP-Trap®_A (Chromotek) coimmunoprecipitation assays were performed as described (65). Samples of unbound and bound proteins (20 μl) were analyzed by immunoblotting using antibodies at the following concentrations: anti-GFP (Santa Cruz), 1:2000; anti-exportin 4 (Abcam), 1:500; anti-exportin 5 (Abcam), 1:2000; anti-exportin 6 (Abcam), 1:1000; anti-exportin 7 (Abcam), 1:1000; horseradish peroxidase (HRP)-conjugated donkey anti-rabbit IgG (GE Healthcare Life Sciences) or mouse anti-goat IgG (Santa Cruz), 1: 25,000.

3 RESULTS

3.1 Overexpression of MED1 increases nuclear retention of TRβ1 and v-ErbA

Although TRα1 and TRβ1 localize primarily to the nucleus at steady state, both receptors rapidly shuttle between the nucleus and cytoplasm (37). The constitutive presence of TR variants in the nucleus points to regulatory factors that promote their nuclear retention.

Given that the Mediator subunit MED1, a transcriptional coactivator, is required for the expression of TR-regulated genes (54,55), we hypothesized that MED1 helps to anchor TR in the nucleus. To test this hypothesis, we employed our well-established, validated approach of transient transfection assays in HeLa (human) cells, which express MED1 and MED13 but do not express detectable levels of TRα1 and TRβ1. Our prior studies have shown that in HeLa cells overexpression of wild-type TR does not saturate the capacity of the nuclear import machinery, nor do fluorescent protein tags alter localization patterns. Further, wild-type TR is primarily nuclear over a wide range of expression levels in transfected cells (35–37,65,69), and supports T_3-dependent gene transactivation in reporter assays (70). Finally, distribution patterns of exogenous TRs in HeLa cells are the same as in cell lines that express endogenous TRs, including HepG2 (hepatocellular carcinoma) cells that express low levels of TRα1 and TRβ1, and GH4C1 (rat pituitary tumor) cells that express high levels of both TRα1 and TRβ1 (70). To determine if increasing levels of MED1 above endogenous levels altered the nucleocytoplasmic distribution patterns of TRα1 and TRβ1, HeLa cells were transfected with either mCherry-tagged TRα1 or TRβ1 alone, or together with GFP-MED1, and the relative nucleus to cytoplasmic (N/C) ratio of fusion protein fluorescence was quantified by fluorescence microscopy. As a negative control, we also performed cotransfections with a truncated form of MED1 (tMED1), which lacks the nuclear receptor-binding boxes, NR-1 and NR-2.

Consistent with previous studies, TRα1 was localized almost entirely to the nucleus, with only a small population of cells (<10%) having a cytosolic population of TRα1 (Fig. 2A); TRβ1 showed a greater cytosolic distribution relative to TRα1 (Fig. 2C) and v-ErbA, the oncogenic homolog of TR, had a predominantly cytoplasmic distribution (Fig. 2E). These differences in distribution patterns of TR variants is thought to result, in part, from the presence of a second NLS, NLS-2, in the A/B domain of TRα1, which is not present in TRβ1 and is mutated in v-ErbA (31) (Fig. 1A). As expected, GFP-MED1 was predominantly nuclear (Fig. 2A, C, E). Interestingly, approximately 50% of the cells transfected with GFP-MED1 alone contained nuclei with discrete fluorescent dots or foci (see Fig. 2E, white arrow); however, when coexpressed with any of the TR variants these nuclear foci were resolved, leading to a diffuse, homogeneous distribution of MED1. When TRα1 and MED 1 were coexpressed, there was no detectable change in TRα1's already primarily nuclear localization ($p=0.299$) (Fig. 2A, B). In contrast, when cotransfected with MED1, there was a striking shift toward significantly greater nuclear localization of TRβ1 ($p=0.004$) (Fig 2C, D) and v-ErbA ($p=0.001$) (Fig 2E, F) with, on average, an approximately 2-fold increase in their relative N/C ratios. Taken together, these data suggest that MED1 promotes nuclear retention of TR and v-ErbA, although the effect on v-ErbA may be indirect, since v-ErbA lacks the AF-2 region present in TR (see Fig. 1). As anticipated, when cotransfected with truncated tMED1, there was no change in localization of TRα1, TRβ1, or v-ErbA (data not shown).

3.2 Knockout of MED1 promotes nuclear export of TRα1 and TRβ1

To further test our model that MED1 plays a pivotal role in nuclear retention of TR subtypes, we examined their intracellular distribution in the presence or absence of MED1. For these experiments, we used established MED1-knockout mouse embryonic fibroblasts (MEFs)

(54). We predicted that a greater cytoplasmic population of TR (lower N/C ratio) would be observed in MED1$^{-/-}$ (null) MEFs compared to MED1$^{+/+}$ (wild-type) MEFs that express endogenous MED1. MED1$^{-/-}$ and MED1$^{+/+}$ MEFs were transfected with expression plasmids for mCherry-tagged TRα1, TRβ1, and v-ErbA, and the nucleocytoplasmic distribution patterns were analyzed. TRα1 (Fig. 3A, B) and TRβ1 (Fig. 3C, D) both showed a marked shift to a more cytosolic population in MEFs lacking MED1. On average, the relative N/C ratio for TRα1 in MED1$^{-/-}$ cells was 1.7-fold lower compared to MED1^{++} cells ($p<0.05$), and the N/C ratio for TRβ1 in MED$^{-/-}$ cells was 2.5-fold lower relative to the distribution pattern in MED1$^{+/+}$ cells ($p<0.001$). These data suggest that in the absence of MED1, nuclear retention of TR is decreased, and more TR is available for nuclear export. As expected, given the primarily cytoplasmic distribution of v-ErbA at steady-state, there was no significant change in localization of v-ErbA in the MED$^{-/-}$ MEFs compared with wild-type MEFs ($p>0.05$) (Fig. 3E, F).

3.3 MED1 differentially impacts the intranuclear dynamics of TR

The reported role of MED1 as a coactivator of TR-regulated genes (41,52,53) led us to hypothesize that overexpressing MED1 would increase TR's residence time bound to DNA or other nuclear factors. As a result, we predicted that overexpression of MED1 would lead to a decrease in TR intranuclear mobility. Prior studies under a variety of conditions have shown that TR is highly dynamic in intranuclear mobility of TRα1 (70,71). First, we examined the intranuclear FRAP profile for TRα1 alone. Given the relatively even, diffuse distribution of TRα1 in the nucleus (see Figs. 2A and 3A), we used a variation of FRAP, termed strip-FRAP, to examine the intranuclear dynamics of TRα1 (66,67). This approach has the advantage of reducing experimental noise by averaging over any heterogeneities in mobility that might exist on a smaller scale (72). In this method, a strip through the nucleus is photobleached and mobility is monitored by the recovery of fluorescent proteins into the bleached strip. Since TR is excluded from nucleoli (dark ovals visible in Fig. 4A); we avoided locating the strip through a nucleolus, although it has been reported that there is no large deviation in the recovery rate of the transcription factor Smad2 around such an obstacle (72). As shown in Fig. 4A, in keeping with our prior studies, TRα1 was highly dynamic in its intranuclear mobility; the calculated half-maximal recovery time ($t_{1/2}$) was 1.01 ± 0.18 sec, with 95% of TRα1 within the mobile fraction.

Next, we compared the intranuclear FRAP profile of cells expressing mCherry-TRα1 to cells coexpressing mCherry-TRα1 and GFP-MED1. For TRα1 coexpressed with MED1, we observed no significant difference in recovery rate, mobile and immobile fractions, half-time slope, and $t_{1/2}$, compared with TRα1 alone (Fig. 4A, B; Table 1). In contrast, when MED1 and TRβ1 were coexpressed, there was a statistically significant reduction in the half-time slope and the estimated half-time; on average, $t_{1/2}$ was 0.92±0.08 sec for TRβ1 alone, compared with 1.20±0.13 sec for TRβ1 coexpressed with MED1. In addition, there was a statistically significant reduction in the mobile fraction, with a concomitant increase in the immobile fraction of TRβ1, from less than 1% to 3.2% immobile (Fig. 4C, D; Table 1).

To place our mobility data for TR from strip-FRAP in context, we also used this approach to determine the intranuclear FRAP profile of the glucocorticoid receptor (GR), which has

been extensively characterized in the literature (73–75). We treated cells expressing GFP-GR (121 kDa) with dexamethasone to induce a nuclear population of GR and then performed strip-FRAP (Fig. 5A, B). While others have reported halftimes of greater than a few seconds for GR, we found that on average, GR's $t_{1/2}$ was ~0.74 sec. However, analysis of individual replicates revealed two distinct populations of GR. One GR population demonstrated a relatively fast halftime (~ 0.6 sec) while the other was much slower (~3.0 sec), a phenomenon that has recently been reported by another group for GR (73). Overall, data from our strip-FRAP experimental approach appears comparable to intranuclear FRAP profiles reported in the literature for other transcription factors.

To examine additional parameters impacting intranuclear mobility, we also used FRAP to analyze a previously constructed expression vector for a fusion protein with NLS-1 in TR's hinge domain (31), termed GFP-GST-GFP-Hinge (Fig. 5C, D). Since the GFP-GST-GFP-Hinge fusion protein lacks the DNA-binding domain present in full-length TR, we predicted that the fusion protein would display greater intranuclear mobility than full-length TR. In support of this prediction, the GFP-GST-GFP-Hinge fusion protein, despite its greater size (87 kDa compared to 73 kDa for GFP-TRα1), had a significantly faster rate of recovery than TRα1 (less than 1.0 sec; $p<0.001$).

3.4 T_3 and EGF alter TRα1 and TRβ1 intranuclear mobility

In prior studies, we did not observe any significant difference between TRα1 shuttling kinetics in the presence or absence of T_3 (39,70); however, we had not previously examined ligand-dependence of intranuclear mobility. Interestingly, in addition to its classic role as an activator of TR-dependent transcription, T_3 also is a potent stimulator of activated MAPK-ERK. HeLa cells express endogenous MED1 and, in HeLa cells, T_3 is capable of triggering MED1 phosphorylation to levels comparable to that observed in cells stimulated with EGF, a well-documented and potent activator of ERK (52). ERK stabilization of MED1 has been shown to correlate with increased TR-dependent transcription; adding EGF and T_3 increases TRE reporter gene transactivation considerably above T_3 alone (53).

To investigate the effect of treatment with T_3 and EGF on the intranuclear mobility of TRα1 and TRβ1, we used strip-FRAP. For mCherry-TRα1, there was no significant difference in the intranuclear FRAP profile in T_3-treated HeLa cells compared to T_3-depleted conditions (Fig.6A, B; Table 1). When cells were treated with EGF, there was a statistically significant decrease of mCherry-TRα1 in the mobile fraction (from 93% to 82%) and a concomitant increase in the immobile fraction (from 7% to 18%); however, there was no statistically significant difference in the overall recovery rate, the half-time slope, and $t_{1/2}$ (Fig. 6A, B; Table 1). In striking contrast, for cells treated with both T_3 and EGF, there was a statistically significant difference in the overall rate of recovery for TRα1, a significant decrease in the mobile fraction (93% to 67%) with a concomitant increase in the immobile fraction (7% to 33%), and a significant difference in the half-time slope (Fig. 6A, B; Table 1). On average, $t_{1/2}$ for TRα1 in the presence of both T_3 and EGF was 3.8 sec, compared with 1.3 sec in their absence. The half-time values were highly variable in the T_3 and EGF-treated cells, however, resulting in no statistical significance.

For mCherry-TRβ1, in T_3-treated cells there was a significant decrease in the overall recovery rate compared with T_3-depleted cells, but there was no significant difference in the mobile and immobile fraction, the half-time slope, or $t_{1/2}$ (Fig.6C, D; Table 1). When cells were treated with EGF, there also was no significant difference in the intranuclear FRAP profile, compared with untreated cells (Fig. 6C, D; Table 1). For mCherry-TRβ-expressing cells treated with both T_3 and EGF, however, there was a dramatic shift in the intranuclear profile; there was a statistically significant difference in the overall rate of recovery, along with a statistically significant increase in the mobile fraction (97% to greater than 99%) with a concomitant decrease in the immobile fraction (3% to less than 1%), and a statistically significant difference in the half-time slope. Finally, there was a statistically significant difference in the half-time value; $t_{1/2}$ shifted from 1.4 sec in T_3-depleted cells to 0.8 sec in T_3/EGF-treated cells (Fig. 6C, D; Table 1). Taken together, these data provide further evidence of the pivotal role played by MED1 in modulating TR intranuclear dynamics. Further, the differential responses to T_3 and EGF by TRα1 and TRβ1 suggest complex interactions with other nuclear factors and signaling pathways, in addition to interaction with unphosphorylated endogenous MED1 and phosphorylated endogenous MED1, induced by T_3/EGF treatment.

3.5 Overexpression of miR-208a alters TR nuclear localization

Another nuclear factor that could contribute to TR nuclear retention is the Mediator subunit MED13. miR-208a is known to downregulate MED13 expression (60), so we predicted that overexpression of miR-208a would lead to great cytosolic population of TRα1, which is primarily nuclear-localized at steady-state under standard conditions (see Fig. 2). When expression plasmids for miR208a and mCherry-TRα1 were cotransfected in HeLa cells, TRα1 showed a significant shift towards the cytosol, compared to cells transfected with scrambled miRNA alone ($p=0.006$) (Fig. 7A), suggesting that downregulation of MED13 by miR208a impacted TRα1 localization. Since these findings pointed to a possible role of MED13 in nuclear retention, we examined the impact of overexpression of MED13 on TRβ1's nucleocytoplasmic distribution and intranuclear mobility. In this case, only TRβ1 was analyzed, since this TR subtype has a small cytosolic population at steady-state (see Fig. 2), and any shift towards greater nuclear localization would be more readily apparent than for TRα1. Cotransfection of an expression plasmid for GFP-MED13 with mCherry-TRβ1, showed no significant impact on its intracellular distribution pattern compared with transfection of TRβ1 alone ($p>0.05$) (Fig. 7B). Finally, TRβ1 alone or coexpressed with MED13, showed no significant differences in its intranuclear FRAP profile ($p>0.05$) (Fig. 7C).

3.6 TR interacts directly with exportins 4, 5, and 7 in its LBD within the MED1-interacting region

The MED1 subunit of the Mediator complex is known to interact with the AF-2 transactivation domain of TR within helix 12 (48). This is particularly intriguing, since our prior studies have shown that AF-2 overlaps with one of TR's nuclear export signals, NES-H12 (31) (see Fig. 1A). Previously, we used RNAi-mediated knockdown to show that exportin 4, exportin 5, and exportin 7 influence TRα1 localization, suggesting these exportins are candidates for mediating TRα1 nuclear export, in combination with the

previously characterized CRM1/calreticulin pathway (34,76). To determine whether these exportins influence localization via direct protein-protein interactions, we performed coimmunoprecipitation assays. Fig. 8 shows western blotting results after coimmunoprecipitation assays for exportin 4, exportin 5, exportin 6 as a control, and exportin 7. Data show that full-length TRα1 interacts directly with exportins 4, 5, and 7 but not exportin 6. Further, we showed that exportins 5 and 7 interact directly with TR's LBD; however, results were inconclusive for exportin 4. These findings suggest that binding of exportins and MED1 to helix 12 of TR could be mutually exclusive, and that MED1 may promote nuclear retention of TR, in part, by blocking this particular export pathway.

4 DISCUSSION

Our long-standing interest is in the complex mechanisms regulating the subcellular distribution of TRα1, TRβ1, and the oncoprotein v-ErbA. Our current working model is one of a finely tuned, dynamic balance among nuclear import, nuclear retention, and nuclear export. Our prior work revealed that TRα1, TRβ1, and the oncoprotein v-ErbA undergo rapid nucleocytoplasmic shuttling (33). Here, our data extend our previous studies on receptor movement to the nucleus, as visualized by FRAP. Recovery half-times of ~1 sec for TRα1 and TRβ1 demonstrate remarkably rapid intranuclear movement, suggesting that TR's association with nuclear factors is dynamic and transient. The results of the current study provide evidence that Mediator subunit MED1 plays a key role in regulating the nuclear retention of TR variants, but that MED13 has a lesser impact. Overexpression of miR-208a, a miRNA that downregulates MED13, shifted TR towards a more cytosolic localization; however, overexpression of MED13 did not lead to increased nuclear localization. These findings could indicate that endogenous levels of MED13 are already at saturating levels for interaction with TR, or that the effects of miR-208a on TR localization involve regulatory pathways separate from MED13. Collectively, MED1 data point to the pivotal role of helix 12 in TR function, with roles in transactivation, ligand binding, and nuclear export. Further, intranuclear mobility of the three variants of TR was differentially influenced by MED1, suggesting that for each variant the balance between nuclear import, nuclear retention, and nuclear export has a different set point, thereby contributing to differential modulation of target genes.

After photobleaching of a region of interest in the nucleus, many transcription factors exhibit complete recoveries within seconds (77), indicating that they can diffuse throughout the entire nucleus and are immobilized to nuclear structures only transiently (70,73). The rapid intranuclear FRAP profiles generated for TR in the current study are thus not without precedent. Intranuclear dynamics are complex, affected by binding interactions, the presence of monomers vs dimers, flow, and inhomogeneity in space (72). Imaging studies of GFP-tagged steroid hormone receptors, including the glucocorticoid receptor, mineralocorticoid receptor, estrogen receptor, and the androgen receptor, have shown changes in intranuclear dynamics affected by a number of factors such as ligand availability, transcriptional activity, and proteasomal activity (78–83). An earlier study of TRβ1 intranuclear mobility by FRAP noted that overexpression of SRC-1, N-CoR1, and HDAC did not affect TRβ1's intranuclear mobility (71); however, when factors retaining unliganded TRβ1 in the nucleus were studied, findings pointed towards a role of N-CoR1 and RXR in maintaining the receptor in

the nucleus (84). Here, we showed that overexpression of MED1 in HeLa cells slows the intranuclear dynamics of TRβ1. MED1 is only found in a small subset of cells (85), however, suggesting a distinct role for MED1 in TR retention for some cell types, but additional mechanisms may be in place to adequately maintain its localization.

We also showed that T_3/EGF treatment, which induces phosphorylation of MED1, alters the intranuclear dynamics of TRα1 and TRβ1, suggesting that the phosphorylation status of MED1 is a key factor in modulating TR intranuclear mobility. Our interest in the impact of phospho-MED1 on TR nuclear retention arose from reports of MED1-stimulated increases in TR-dependent transcription (53). Importantly, MED1 phosphorylation also leads to the upregulation of MED1 by increasing its stability and half-life, which ultimately contributes to the development and progression of several types of cancer, including breast, lung, cervical, and prostate cancer. (52,53,86–94). Countering this upregulation, MED1 concentration and phosphorylation are surveilled by miR-205, which downregulates MED1 expression. By stabilizing the half-life of MED1 through T_3 and EGF-induced phosphorylation in our experiments, we may also have been simultaneously inducing upregulation of endogenous miR-205, and rapid degradation of endogenous phospho-MED1 (86). Differences in levels of endogenous miR-205 and concomitant MED1 turnover between biological replicates could explain some of the variability we observed in the intranuclear FRAP profiles for TR in T_3 and EGF-treated cells (see Table 1).

One of our intriguing observations in the current study was that approximately 50% of the cells transfected with GFP-MED1 alone contained nuclei with discrete fluorescent dots or foci. When coexpressed with any of the TR variants these nuclear foci were resolved, leading to a diffuse, homogeneous distribution of MED1. There is precedence in the literature for dynamic changes in protein distribution in the nucleus. For example, the nuclear corepressor N-CoR is redistributed into intranuclear foci together with steroid hormone receptors in the presence of agonist, and its mobility is significantly decreased (95). Of more direct relevance to the current study, recently, it has been shown that Mediator exists in two states: a population of transient small (~100 nm) clusters with an average lifetime of 11 sec, and larger, temporally stable clusters of Mediator and RNA polymerase II (>300 nm) which associate with chromatin. These clusters have properties of phase-separated condensates, and may facilitate long-range interactions between enhancers and promoters (46). MED1 also was found to occupy discrete nuclear bodies that occur at “super-enhancers,” clusters of enhancers that are bound with a very high density of interacting factors. The MED1 nuclear bodies show rapid recovery of fluorescence after photobleaching and the large intrinsically disordered regions of MED1 form phase-separated liquid droplets *in vitro*, suggesting that MED1 may contribute to the compartmentalization and concentration of biochemical reactions associated with transcription (96). Diverse transcription factors may thus interact with subunits of Mediator through the phase-separating capacity of their intrinsically disordered activation domains, leading to gene activation (97). Such a general mechanism also could apply to the interactions of TR with MED1 through the helix 12 activation domain.

TRα1 and TRβ1 have multiple NESs in their LBD (see Fig. 1). One of these, NES-H12, is naturally deleted from v-ErbA (31). Extrapolating from our coimmunoprecipitation results

showing direct interaction between various exportins and the LBD of TRα1, we propose a model involving competition between MED1 and exportins 5 and 7 to balance nuclear retention and export of TR. By removing MED1 from this competition in MED1$^{-/-}$ knockout MEFs, it is plausible that the greater cytoplasmic distribution of TR relative to MED1$^{+/+}$ MEFs that we observed is due to increased interaction between NES-H12 of TRα1 and TRβ1 and exportins 5 and 7. Additional analysis of competition for binding TR by exportins and MED1 should help to confirm and extend this model, and enhance understanding of how the dual functionality of helix 12 in TR's LBD serves to modulate both gene transactivation and nuclear export.

ACKNOWLEDGMENTS

This work was supported by Grant 2R15DK058028 from the National Institutes of Health and Grant MCB120513 from the National Science Foundation (to L.A.A). We thank Dr. Robert Roeder (Rockefeller University) for generously providing the MED1^{++} (Trap220^{++}) and MED1$^{-/-}$ (Trap220$^{-/-}$) MEFs, and Drs. Abigail Reft and Michael D. LaMar (College of William & Mary) for assistance with confocal microscopy training and FRAP quantification, respectively.

REFERENCES

1. Mullur R, Liu YY, Brent GA. Thyroid hormone regulation of metabolism. Physiol Rev 2014; 94:355–382 [PubMed: 24692351]
2. Flamant F, Gauthier K. Thyroid hormone receptors: the challenge of elucidating isotype-specific functions and cell-specific response. Biochim Biophys Acta 2013; 1830:3900–3907 [PubMed: 22704954]
3. Dinda S, Sanchez A, Moudgil V. Estrogen-like effects of thyroid hormone on the regulation of tumor suppressor proteins, p53 and retinoblastoma, in breast cancer cells. Oncogene 2002; 21:761–768 [PubMed: 11850804]
4. Puzianowska-Kuznicka M, Pietrzak M, Turowska O, Nauman A. Thyroid hormones and their receptors in the regulation of cell proliferation. Acta biochimica Polonica 2006; 53:641–650 [PubMed: 17115080]
5. Qi JS, Yuan Y, Desai-Yajnik V, Samuels HH. Regulation of the mdm2 oncogene by thyroid hormone receptor. Molecular and cellular biology 1999; 19:864–872 [PubMed: 9858609]
6. Pascual A, Aranda A. Thyroid hormone receptors, cell growth and differentiation. Biochim Biophys Acta 2013; 1830:3908–3916 [PubMed: 22484490]
7. Preau L, Fini JB, Morvan-Dubois G, Demeneix B. Thyroid hormone signaling during early neurogenesis and its significance as a vulnerable window for endocrine disruption. Biochim Biophys Acta 2014;
8. Tata JR. The road to nuclear receptors of thyroid hormone. Biochim Biophys Acta 2013; 1830:3860–3866 [PubMed: 22450156]
9. Wojcicka A, Bassett JH, Williams GR. Mechanisms of action of thyroid hormones in the skeleton. Biochim Biophys Acta 2013; 1830:3979–3986 [PubMed: 22634735]
10. Contreras-Jurado C, Garcia-Serrano L, Martinez-Fernandez M, Ruiz-Llorente L, Paramio JM, Aranda A. Impaired hair growth and wound healing in mice lacking thyroid hormone receptors. PloS one 2014; 9:e108137 [PubMed: 25254665]
11. Vella KR, Ramadoss P, Costa ESRH, Astapova I, Ye FD, Holtz KA, Harris JC, Hollenberg AN. Thyroid hormone signaling in vivo requires a balance between coactivators and corepressors. Molecular and cellular biology 2014; 34:1564–1575 [PubMed: 24550004]
12. Diallo EM, Wilhelm KG Jr., Thompson DL, Koenig RJ. Variable RXR requirements for thyroid hormone responsiveness of endogenous genes. Molecular and cellular endocrinology 2007; 264:149–156 [PubMed: 17161906]
13. Morte B, Bernal J. Thyroid hormone action: astrocyte-neuron communication. Frontiers in endocrinology 2014; 5:82 [PubMed: 24910631]

14. Horlein AJ, Naar AM, Heinzel T, Torchia J, Gloss B, Kurokawa R, Ryan A, Kamei Y, Soderstrom M, Glass CK, et al. Ligand-independent repression by the thyroid hormone receptor mediated by a nuclear receptor co-repressor. Nature 1995; 377:397–404 [PubMed: 7566114]
15. Sun Z, Feng D, Fang B, Mullican SE, You SH, Lim HW, Everett LJ, Nabel CS, Li Y, Selvakumaran V, Won KJ, Lazar MA. Deacetylase-independent function of HDAC3 in transcription and metabolism requires nuclear receptor corepressor. Molecular cell 2013; 52:769–782 [PubMed: 24268577]
16. Rosen MD, Privalsky ML. Thyroid hormone receptor mutations in cancer and resistance to thyroid hormone: perspective and prognosis. Journal of thyroid research 2011; 2011:361304 [PubMed: 21760978]
17. Rosen MD, Privalsky ML. Thyroid hormone receptor mutations found in renal clear cell carcinomas alter corepressor release and reveal helix 12 as key determinant of corepressor specificity. Mol Endocrinol 2009; 23:1183–1192 [PubMed: 19407221]
18. Figueira AC, Saidemberg DM, Souza PC, Martinez L, Scanlan TS, Baxter JD, Skaf MS, Palma MS, Webb P, Polikarpov I. Analysis of agonist and antagonist effects on thyroid hormone receptor conformation by hydrogen/deuterium exchange. Mol Endocrinol 2011; 25:15–31 [PubMed: 21106879]
19. Dasgupta S, O'Malley BW. Transcriptional coregulators: emerging roles of SRC family of coactivators in disease pathology. Journal of molecular endocrinology 2014; 53:R47–59 [PubMed: 25024406]
20. Soriano FX, Leveille F, Papadia S, Bell KF, Puddifoot C, Hardingham GE. Neuronal activity controls the antagonistic balance between peroxisome proliferator-activated receptor-gamma coactivator-1alpha and silencing mediator of retinoic acid and thyroid hormone receptors in regulating antioxidant defenses. Antioxidants & redox signaling 2011; 14:1425–1436 [PubMed: 20849372]
21. Astapova I, Hollenberg AN. The in vivo role of nuclear receptor corepressors in thyroid hormone action. Biochim Biophys Acta 2013; 1830:3876–3881 [PubMed: 22801336]
22. Astapova I, Vella KR, Ramadoss P, Holtz KA, Rodwin BA, Liao XH, Weiss RE, Rosenberg MA, Rosenzweig A, Hollenberg AN. The nuclear receptor corepressor (NCoR) controls thyroid hormone sensitivity and the set point of the hypothalamic-pituitary-thyroid axis. Mol Endocrinol 2011; 25:212–224 [PubMed: 21239618]
23. Brent GA. Mechanisms of thyroid hormone action. J Clin Invest 2012; 122:3035–3043 [PubMed: 22945636]
24. Adams RL, Wente SR. Uncovering nuclear pore complexity with innovation. Cell 2013; 152:1218–1221 [PubMed: 23498931]
25. Cook A, Bono F, Jinek M, Conti E. Structural Biology of Nucleocytoplasmic Transport. Annu Rev Biochem 2007; 76:647 LP–671 [PubMed: 17506639]
26. Gorlich D, Kutay U. Transport between the cell nucleus and the cytoplasm. Annu Rev Cell Dev Biol 1999; 15:607–660 [PubMed: 10611974]
27. Tetenbaum-Novatt J, Rout MP. The mechanism of nucleocytoplasmic transport through the nuclear pore complex. Cold Spring Harb Symp Quant Biol 2010; 75:567–584 [PubMed: 21447814]
28. Stewart M Molecular mechanism of the nuclear protein import cycle. Nat Rev Mol Cell Biol 2007; 8:195–208 [PubMed: 17287812]
29. Grossman E, Medalia O, Zwerger M. Functional architecture of the nuclear pore complex. Annu Rev Biophys 2012; 41:557–584 [PubMed: 22577827]
30. Gorlich D, Mattaj IW. Nucleocytoplasmic transport. Science 1996; 271:1513–1518 [PubMed: 8599106]
31. Mavinakere MS, Powers JM, Subramanian KS, Roggero VR, Allison LA. Multiple novel signals mediate thyroid hormone receptor nuclear import and export. J Biol Chem 2012; 287:31280–31297 [PubMed: 22815488]
32. Anyetei-Anum CS, Roggero VR, Allison LA. Thyroid hormone receptor localization in target tissues. J Endocrinol 2018;
33. Zhang J, Roggero VR, Allison LA. Nuclear Import and Export of the Thyroid Hormone Receptor. Vitam Horm 2018; 106:45–66 [PubMed: 29407444]

34. Subramanian KS, Dziedzic RC, Nelson HN, Stern ME, Roggero VR, Bondzi C, Allison LA. Multiple exportins influence thyroid hormone receptor localization. Molecular and cellular endocrinology 2015; 411:86–96 [PubMed: 25911113]
35. Bonamy GM, Guiochon-Mantel A, Allison LA. Cancer promoted by the oncoprotein v-ErbA may be due to subcellular mislocalization of nuclear receptors. Mol Endocrinol 2005; 19:1213–1230 [PubMed: 15650025]
36. Bondzi C, Brunner AM, Munyikwa MR, Connor CD, Simmons AN, Stephens SL, Belt PA, Roggero VR, Mavinakere MS, Hinton SD, Allison LA. Recruitment of the oncoprotein v-ErbA to aggresomes. Molecular and cellular endocrinology 2011; 332:196–212 [PubMed: 21075170]
37. Bunn CF, Neidig JA, Freidinger KE, Stankiewicz TA, Weaver BS, McGrew J, Allison LA. Nucleocytoplasmic shuttling of the thyroid hormone receptor alpha. Mol Endocrinol 2001; 15:512–533 [PubMed: 11266504]
38. DeLong LJ, Bonamy GM, Fink EN, Allison LA. Nuclear export of the oncoprotein v-ErbA is mediated by acquisition of a viral nuclear export sequence. J Biol Chem 2004; 279:15356–15367 [PubMed: 14729678]
39. Grespin ME, Bonamy GM, Roggero VR, Cameron NG, Adam LE, Atchison AP, Fratto VM, Allison LA. Thyroid hormone receptor alpha 1 follows a cooperative CRM1/calreticulin-mediated nuclear export pathway. J Biol Chem 2008;
40. Chong S, Dugast-Darzacq C, Liu Z, Dong P, Dailey GM, Cattoglio C, Heckert A, Banala S, Lavis L, Darzacq X, Tjian R. Imaging dynamic and selective low-complexity domain interactions that control gene transcription. Science 2018; 361
41. Fondell JD. The Mediator complex in thyroid hormone receptor action. Biochim Biophys Acta 2013; 1830:3867–3875 [PubMed: 22402254]
42. Poss ZC, Ebmeier CC, Taatjes DJ. The Mediator complex and transcription regulation. Critical reviews in biochemistry and molecular biology 2013; 48:575–608 [PubMed: 24088064]
43. Napoli C, Sessa M, Infante T, Casamassimi A. Unraveling framework of the ancestral Mediator complex in human diseases. Biochimie 2012; 94:579–587 [PubMed: 21983542]
44. Nozawa K, Schneider TR, Cramer P. Core Mediator structure at 3.4 A extends model of transcription initiation complex. Nature 2017; 545:248–251 [PubMed: 28467824]
45. Tsai KL, Yu X, Gopalan S, Chao TC, Zhang Y, Florens L, Washburn MP, Murakami K, Conaway RC, Conaway JW, Asturias FJ. Mediator structure and rearrangements required for holoenzyme formation. Nature 2017; 544:196–201 [PubMed: 28241144]
46. Cho WK, Spille JH, Hecht M, Lee C, Li C, Grube V, Cisse, II. Mediator and RNA polymerase II clusters associate in transcription-dependent condensates. Science 2018; 361:412–415 [PubMed: 29930094]
47. Fondell JD, Brunel F, Hisatake K, Roeder RG. Unliganded thyroid hormone receptor alpha can target TATA-binding protein for transcriptional repression. Molecular and cellular biology 1996; 16:281–287 [PubMed: 8524305]
48. Ren Y, Behre E, Ren Z, Zhang J, Wang Q, Fondell JD. Specific structural motifs determine TRAP220 interactions with nuclear hormone receptors. Molecular and cellular biology 2000; 20:5433–5446 [PubMed: 10891484]
49. Yuan CX, Ito M, Fondell JD, Fu ZY, Roeder RG. The TRAP220 component of a thyroid hormone receptor-associated protein (TRAP) coactivator complex interacts directly with nuclear receptors in a ligand-dependent fashion. Proc Natl Acad Sci U S A 1998; 95:7939–7944 [PubMed: 9653119]
50. Ge K, Cho YW, Guo H, Hong TB, Guermah M, Ito M, Yu H, Kalkum M, Roeder RG. Alternative mechanisms by which mediator subunit MED1/TRAP220 regulates peroxisome proliferator-activated receptor gamma-stimulated adipogenesis and target gene expression. Molecular and cellular biology 2008; 28:1081–1091 [PubMed: 18039840]
51. Broekema MF, Hollman DAA, Koppen A, van den Ham HJ, Melchers D, Pijnenburg D, Ruijtenbeek R, van Mil SWC, Houtman R, Kalkhoven E. Profiling of 3696 Nuclear Receptor-Coregulator Interactions: A Resource for Biological and Clinical Discovery. Endocrinology 2018; 159:2397–2407 [PubMed: 29718163]

52. Belakavadi M, Pandey PK, Vijayvargia R, Fondell JD. MED1 phosphorylation promotes its association with mediator: implications for nuclear receptor signaling. Molecular and cellular biology 2008; 28:3932–3942 [PubMed: 18391015]
53. Pandey PK, Udayakumar TS, Lin X, Sharma D, Shapiro PS, Fondell JD. Activation of TRAP/mediator subunit TRAP220/Med1 is regulated by mitogen-activated protein kinase-dependent phosphorylation. Molecular and cellular biology 2005; 25:10695–10710 [PubMed: 16314496]
54. Ito M, Yuan CX, Okano HJ, Darnell RB, Roeder RG. Involvement of the TRAP220 component of the TRAP/SMCC coactivator complex in embryonic development and thyroid hormone action. Molecular cell 2000; 5:683–693 [PubMed: 10882104]
55. Malik S, Guermah M, Yuan CX, Wu W, Yamamura S, Roeder RG. Structural and functional organization of TRAP220, the TRAP/mediator subunit that is targeted by nuclear receptors. Molecular and cellular biology 2004; 24:8244–8254 [PubMed: 15340084]
56. Diniz GP, Takano AP, Barreto-Chaves ML. MiRNA-208a and miRNA-208b are triggered in thyroid hormone-induced cardiac hypertrophy - role of type 1 Angiotensin II receptor (AT1R) on miRNA-208a/alpha-MHC modulation. Molecular and cellular endocrinology 2013; 374:117–124 [PubMed: 23623871]
57. Prado-Uribe MD, Soto-Abraham MV, Mora-Villalpando CJ, Gallardo JM, Bonilla E, Avila M, Tena E, Paniagua R. Role of thyroid hormones and mir-208 in myocardial remodeling in 5/6 nephrectomized rats. Archives of medical research 2013; 44:616–622 [PubMed: 24246300]
58. Small EM, Olson EN. Pervasive roles of microRNAs in cardiovascular biology. Nature 2011; 469:336–342 [PubMed: 21248840]
59. Khakhina S, Cooper KF, Strich R. Med13p prevents mitochondrial fission and programmed cell death in yeast through nuclear retention of cyclin C. Molecular biology of the cell 2014; 25:2807–2816 [PubMed: 25057017]
60. Grueter CE, van Rooij E, Johnson BA, DeLeon SM, Sutherland LB, Qi X, Gautron L, Elmquist JK, Bassel-Duby R, Olson EN. A cardiac microRNA governs systemic energy homeostasis by regulation of MED13. Cell 2012; 149:671–683 [PubMed: 22541436]
61. Schiano C, Casamassimi A, Vietri MT, Rienzo M, Napoli C. The roles of mediator complex in cardiovascular diseases. Biochim Biophys Acta 2014; 1839:444–451 [PubMed: 24751643]
62. Amoasii L, Holland W, Sanchez-Ortiz E, Baskin KK, Pearson M, Burgess SC, Nelson BR, Bassel-Duby R, Olson EN. A MED13-dependent skeletal muscle gene program controls systemic glucose homeostasis and hepatic metabolism. Genes Dev 2016; 30:434–446 [PubMed: 26883362]
63. Petrenko N, Jin Y, Wong KH, Struhl K. Mediator Undergoes a Compositional Change during Transcriptional Activation. Molecular cell 2016; 64:443–454 [PubMed: 27773675]
64. Belakavadi M, Fondell JD. Cyclin-dependent kinase 8 positively cooperates with Mediator to promote thyroid hormone receptor-dependent transcriptional activation. Molecular and cellular biology 2010; 30:2437–2448 [PubMed: 20231357]
65. Roggero VR, Zhang J, Parente LE, Doshi Y, Dziedzic RC, McGregor EL, Varjabedian AD, Schad SE, Bondzi C, Allison LA. Nuclear import of the thyroid hormone receptor alpha1 is mediated by importin 7, importin beta1, and adaptor importin alpha1. Mol Cell Endocrinol 2016; 419:185–197 [PubMed: 26525414]
66. Weiss M Challenges and artifacts in quantitative photobleaching experiments. Traffic 2004; 5:662–671 [PubMed: 15296491]
67. Yang J, Kohler K, Davis DM, Burroughs NJ. An improved strip FRAP method for estimating diffusion coefficients: correcting for the degree of photobleaching. J Microsc 2010; 238:240–253 [PubMed: 20579262]
68. Phair RD, Gorski SA, Misteli T. Measurement of dynamic protein binding to chromatin in vivo, using photobleaching microscopy. Methods Enzymol 2004; 375:393–414 [PubMed: 14870680]
69. Anyetei-Anum CS, Roggero VR, Allison LA. Thyroid hormone receptor localization in target tissues. J Endocrinol 2018; 237:R19–R34 [PubMed: 29440347]
70. Anyetei-Anum CS, Evans RM, Back AM, Roggero VR, Allison LA. Acetylation modulates thyroid hormone receptor intracellular localization and intranuclear mobility. Mol Cell Endocrinol 2019; 495:110509 [PubMed: 31319097]

71. Maruvada P, Baumann CT, Hager GL, Yen PM. Dynamic Shuttling and Intranuclear Mobility of Nuclear Hormone Receptors. Journal of Biological Chemistry 2003; 278:12425–12432 [PubMed: 12506123]
72. Gonzalez-Perez V, Schmierer B, Hill CS, Sear RP. Studying Smad2 intranuclear diffusion dynamics by mathematical modelling of FRAP experiments. Integr Biol (Camb) 2011; 3:197–207 [PubMed: 21240396]
73. Groeneweg FL, van Royen ME, Fenz S, Keizer VI, Geverts B, Prins J, de Kloet ER, Houtsmuller AB, Schmidt TS, Schaaf MJ. Quantitation of glucocorticoid receptor DNA-binding dynamics by single-molecule microscopy and FRAP. PloS one 2014; 9:e90532 [PubMed: 24632838]
74. Meijsing SH, Elbi C, Luecke HF, Hager GL, Yamamoto KR. The ligand binding domain controls glucocorticoid receptor dynamics independent of ligand release. Molecular and cellular biology 2007; 27:2442–2451 [PubMed: 17261597]
75. Carrero G, McDonald D, Crawford E, de Vries G, Hendzel MJ. Using FRAP and mathematical modeling to determine the in vivo kinetics of nuclear proteins. Methods 2003; 29:14–28 [PubMed: 12543068]
76. Grespin ME, Bonamy GM, Roggero VR, Cameron NG, Adam LE, Atchison AP, Fratto VM, Allison LA. Thyroid hormone receptor alpha1 follows a cooperative CRM1/calreticulin-mediated nuclear export pathway. J Biol Chem 2008; 283:25576–25588 [PubMed: 18641393]
77. Mueller F, Morisaki T, Mazza D, McNally JG. Minimizing the impact of photoswitching of fluorescent proteins on FRAP analysis. Biophysical journal 2012; 102:1656–1665 [PubMed: 22500766]
78. Nishi M, Noriko HH, Kawata M. Intranuclear dynamics of corticosteroid receptors and effects of proteasomal activity in cultured hippocampal neural cells. Neurosci Lett 2011; 494:65–69 [PubMed: 21362454]
79. Tanida T, Matsuda KI, Yamada S, Hashimoto T, Kawata M. Estrogen-related Receptor beta Reduces the Subnuclear Mobility of Estrogen Receptor alpha and Suppresses Estrogen-dependent Cellular Function. J Biol Chem 2015; 290:12332–12345 [PubMed: 25805499]
80. Htun H, Holth LT, Walker D, Davie JR, Hager GL. Direct visualization of the human estrogen receptor alpha reveals a role for ligand in the nuclear distribution of the receptor. Molecular biology of the cell 1999; 10:471–486 [PubMed: 9950689]
81. Stenoien DL, Patel K, Mancini MG, Dutertre M, Smith CL, O'Malley BW, Mancini MA. FRAP reveals that mobility of oestrogen receptor-alpha is ligand- and proteasome-dependent. Nat Cell Biol 2001; 3:15–23 [PubMed: 11146621]
82. Ochiai I, Matsuda K, Nishi M, Ozawa H, Kawata M. Imaging analysis of subcellular correlation of androgen receptor and estrogen receptor alpha in single living cells using green fluorescent protein color variants. Mol Endocrinol 2004; 18:26–42 [PubMed: 14563933]
83. Hashimoto T, Matsuda K, Kawata M. Scaffold attachment factor B (SAFB)1 and SAFB2 cooperatively inhibit the intranuclear mobility and function of ERalpha. J Cell Biochem 2012; 113:3039–3050 [PubMed: 22566185]
84. Baumann CT, Maruvada P, Hager GL, Yen PM. Nuclear Cytoplasmic Shuttling by Thyroid Hormone Receptors. J Biol Chem 2001; 276:11237–11245 [PubMed: 11152480]
85. Zhang X, Krutchinsky A, Fukuda A, Chen W, Yamamura S, Chait BT, Roeder RG. MED1/TRAP220 exists predominantly in a TRAP/ Mediator subpopulation enriched in RNA polymerase II and is required for ER-mediated transcription. Molecular cell 2005; 19:89–100 [PubMed: 15989967]
86. Jin F, Irshad S, Yu W, Belakavadi M, Chekmareva M, Ittmann MM, Abate-Shen C, Fondell JD. ERK and AKT signaling drive MED1 overexpression in prostate cancer in association with elevated proliferation and tumorigenicity. Mol Cancer Res 2013; 11:736–747 [PubMed: 23538858]
87. Vijayvargia R, May MS, Fondell JD. A coregulatory role for the mediator complex in prostate cancer cell proliferation and gene expression. Cancer Res 2007; 67:4034–4041 [PubMed: 17483314]
88. Kim HJ, Yun J. Checkpoint-dependent phosphorylation of Med1/TRAP220 in response to DNA damage. Acta Biochim Biophys Sin (Shanghai) 2017; 49:496–502 [PubMed: 28430840]

89. Chen Z, Zhang C, Wu D, Chen H, Rorick A, Zhang X, Wang Q. Phospho-MED1-enhanced UBE2C locus looping drives castration-resistant prostate cancer growth. EMBO J 2011; 30:2405–2419 [PubMed: 21556051]

90. Cui Y, Zhang M, Pestell R, Curran EM, Welshons WV, Fuqua SA. Phosphorylation of estrogen receptor alpha blocks its acetylation and regulates estrogen sensitivity. Cancer Res 2004; 64:9199–9208 [PubMed: 15604293]

91. Kim HJ, Roh MS, Son CH, Kim AJ, Jee HJ, Song N, Kim M, Seo SY, Yoo YH, Yun J. Loss of Med1/TRAP220 promotes the invasion and metastasis of human non-small-cell lung cancer cells by modulating the expression of metastasis-related genes. Cancer Lett 2012; 321:195–202 [PubMed: 22342682]

92. Hulf T, Sibbritt T, Wiklund ED, Patterson K, Song JZ, Stirzaker C, Qu W, Nair S, Horvath LG, Armstrong NJ, Kench JG, Sutherland RL, Clark SJ. Epigenetic-induced repression of microRNA-205 is associated with MED1 activation and a poorer prognosis in localized prostate cancer. Oncogene 2013; 32:2891–2899 [PubMed: 22869146]

93. Mouillet JF, Chu T, Nelson DM, Mishima T, Sadovsky Y. MiR-205 silences MED1 in hypoxic primary human trophoblasts. FASEB J 2010; 24:2030–2039 [PubMed: 20065103]

94. Xie H, Zhao Y, Caramuta S, Larsson C, Lui WO. miR-205 expression promotes cell proliferation and migration of human cervical cancer cells. PloS one 2012; 7:e46990 [PubMed: 23056551]

95. Wu Y, Kawate H, Ohnaka K, Nawata H, Takayanagi R. Nuclear compartmentalization of N-CoR and its interactions with steroid receptors. Molecular and cellular biology 2006; 26:6633–6655 [PubMed: 16914745]

96. Sabari BR, Dall'Agnese A, Boija A, Klein IA, Coffey EL, Shrinivas K, Abraham BJ, Hannett NM, Zamudio AV, Manteiga JC, Li CH, Guo YE, Day DS, Schuijers J, Vasile E, Malik S, Hnisz D, Lee TI, Cisse, II, Roeder RG, Sharp PA, Chakraborty AK, Young RA. Coactivator condensation at super-enhancers links phase separation and gene control. Science 2018; 361

97. Boija A, Klein IA, Sabari BR, Dall'Agnese A, Coffey EL, Zamudio AV, Li CH, Shrinivas K, Manteiga JC, Hannett NM, Abraham BJ, Afeyan LK, Guo YE, Rimel JK, Fant CB, Schuijers J, Lee TI, Taatjes DJ, Young RA. Transcription Factors Activate Genes through the Phase-Separation Capacity of Their Activation Domains. Cell 2018;

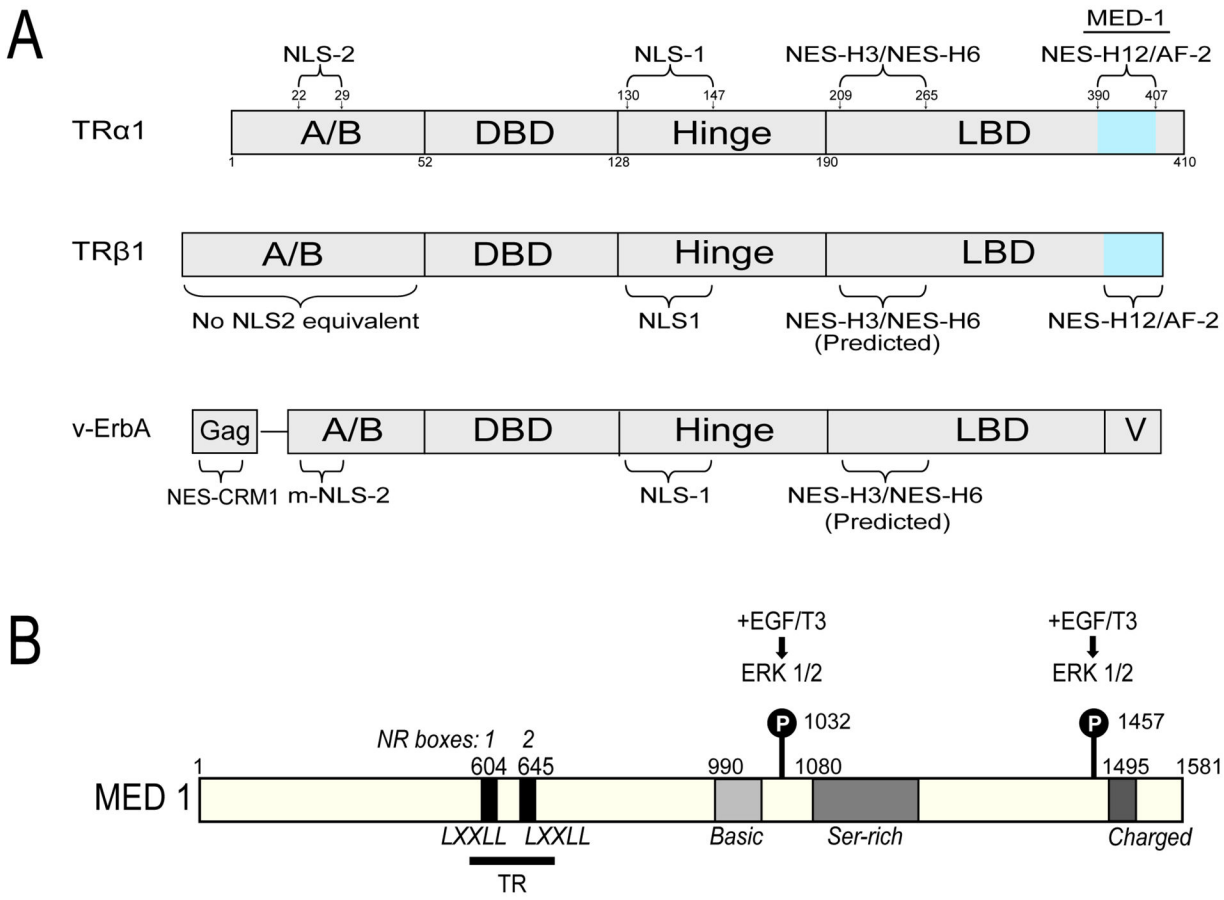

FIGURE 1.

Functional domains in thyroid hormone receptor (TR) major subtypes and MED1. (A) Domain structures of TRα1, TRβ1, and v-ErbA (not to scale). The positions of nuclear localization signal (NLS) and nuclear export signal (NES) motifs are indicated in relation to the respective individual domains of TRα1 (31). Abbreviations are as follows: A/B, A/B domain; DBD, DNA-binding domain; Hinge, hinge domain; LBD, ligand-binding domain; AF-2; activation function 2; NES-CRM1, CRM1-dependent NES in the viral Gag region of v-ErbA; m-NLS, inactive NLS-2 equivalent in v-ErbA; NES-H3/H6 (Predicted), based on the sequence identity with NES-H3 and NES-H6 in TRα1; V, v-ErbA-specific C-terminal sequence that lacks the NES-H12/AF-2 region. (B) Regions of MED1 identified for interaction with TR (41). LXXLL motifs at residues 604 (NR box 1) and 645 (NR box 2) identify the point of contact between TRα1 and MED1. Threonine (Thr)-1032 and Thr-1457 are phosphorylated by MAPK-ERK when stimulated by EGF and/or T_3 (52,53).

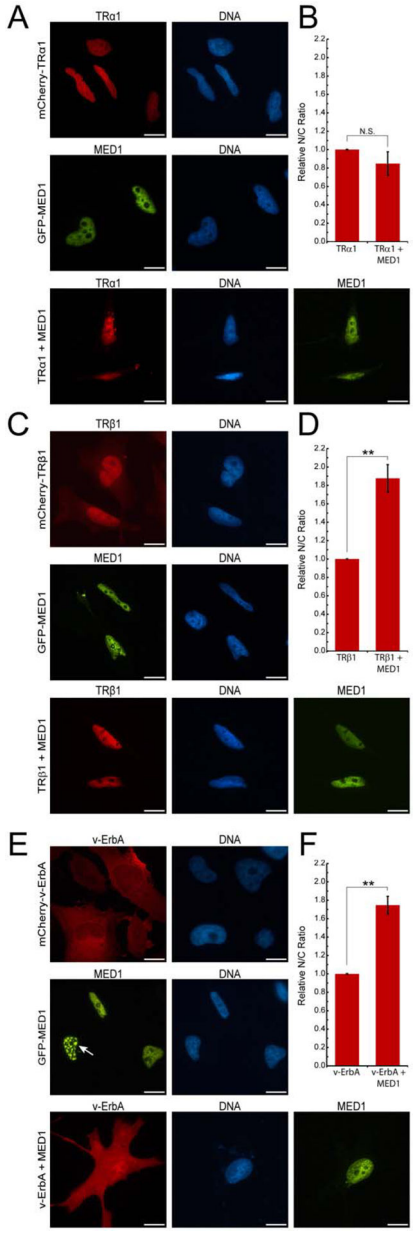

FIGURE 2.

Overexpression of MED1 differentially affects the nucleocytoplasmic distribution of TR subtypes. (A) HeLa cells transfected with mCherry-TRα1 expression plasmid or cotransfected with mCherry-TRα1 and GFP-MED1 expression plasmids, as indicated, were analyzed by fluorescence microscopy after staining with DAPI to visualize the nucleus. Scale bar = 10 μm. (B) Bars indicate the relative nuclear to cytoplasmic (N/C) fluorescence ratio for TRα1 (average N/C ratio in cotransfected cells normalized to the N/C ratio in single-transfected cells). Error bars indicate ±SEM. Cotransfection with MED1 yielded no change in intracellular distribution of TRα1, compared with TRα1 alone (N/C=1.0; N.S., $p>0.05$; n=3 separate, biologically independent replicates; 100 cells per replicate). (C) HeLa cells were transfected with either mCherry-TRβ1 expression plasmids, or cotransfected with

mCherry-TRβ1 and GFP-tagged MED1 expression plasmids, as indicated. (D) Cotransfection with MED1 significantly increased the nuclear localization of TRβ1, compared to transfection of TRβ1 alone (N/C>1.0; **, $p<0.01$). (E) HeLa cells were transfected with either mCherry-v-ErbA expression plasmids, or cotransfected with mCherry-v-ErbA and GFP-MED1 expression plasmids, as indicated. (F) Cotransfection with MED1 significantly increased the nuclear localization of v-ErbA, compared to transfection with v-ErbA alone (N/C>1.0; **, $p<0.01$).

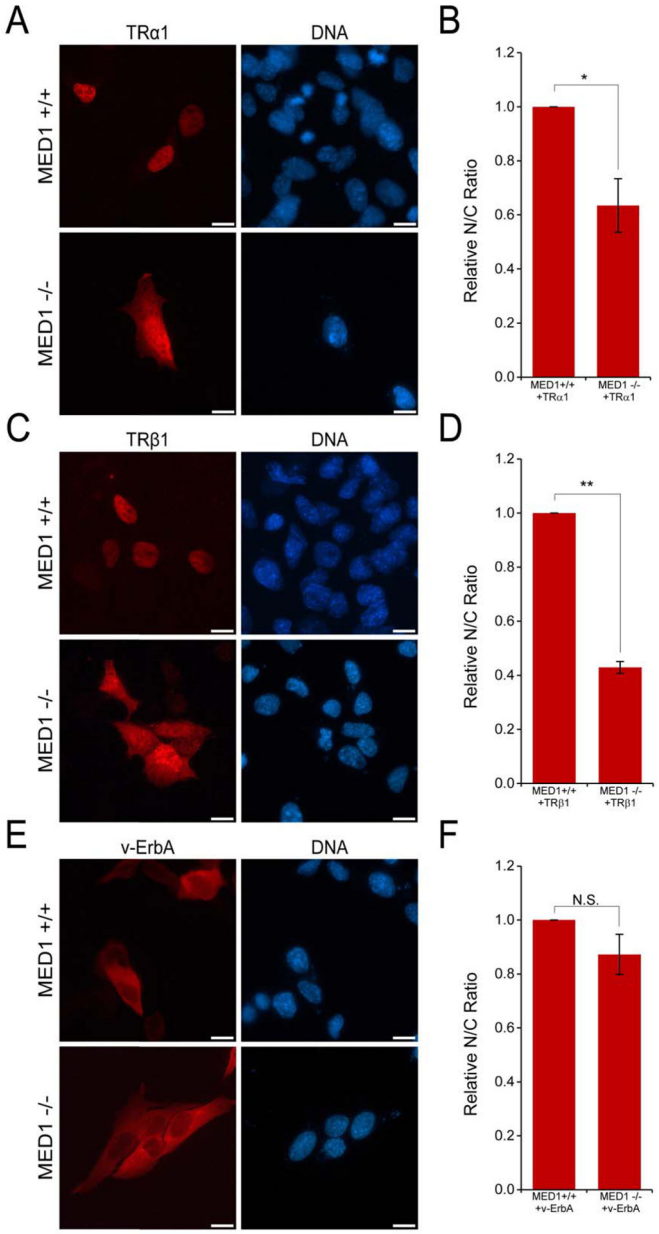

FIGURE 3.

Knockout of MED1 decreases the nuclear retention of TRα1 and TRβ1. (A) MED1$^{-/-}$ and MED$^{+/+}$ cells, as indicated, were transfected with mCherry-TRα1 expression plasmids and analyzed using fluorescence microscopy, after staining with DAPI to visualize the nucleus. Scale bar = 10 μm. (B) Bars indicate the relative nuclear to cytoplasmic (N/C) fluorescence ratio for TRα1 (average N/C ratio in MED1$^{-/-}$ cells normalized to the N/C ratio in MED$^{+/+}$ cells). Error bars indicate ±SEM. TRα1 is shifted toward a more cytoplasmic distribution in MED1$^{-/-}$ cells, compared to MED$^{+/+}$ cells (N/C<1.0; *, p<0.05). (C) MED1$^{-/-}$ and MED$^{+/+}$ cells, as indicated, were transfected with mCherry-TRβ1 expression plasmids and analyzed by fluorescence microscopy. (D) TRβ1 is shifted toward a more cytoplasmic distribution in MED1$^{-/-}$ cells, compared to MED$^{+/+}$ cells (N/C<1.0; **, p=0.001). (E) MED1$^{-/-}$ and MED

$^{+/+}$ cells, as indicated, were transfected with mCherry-v-ErbA expression plasmids and analyzed by fluorescence microscopy. (F) Knockout of MED1 has no effect on the nuclear retention of v-ErbA (N/C=1.0; N.S., p>0.05).

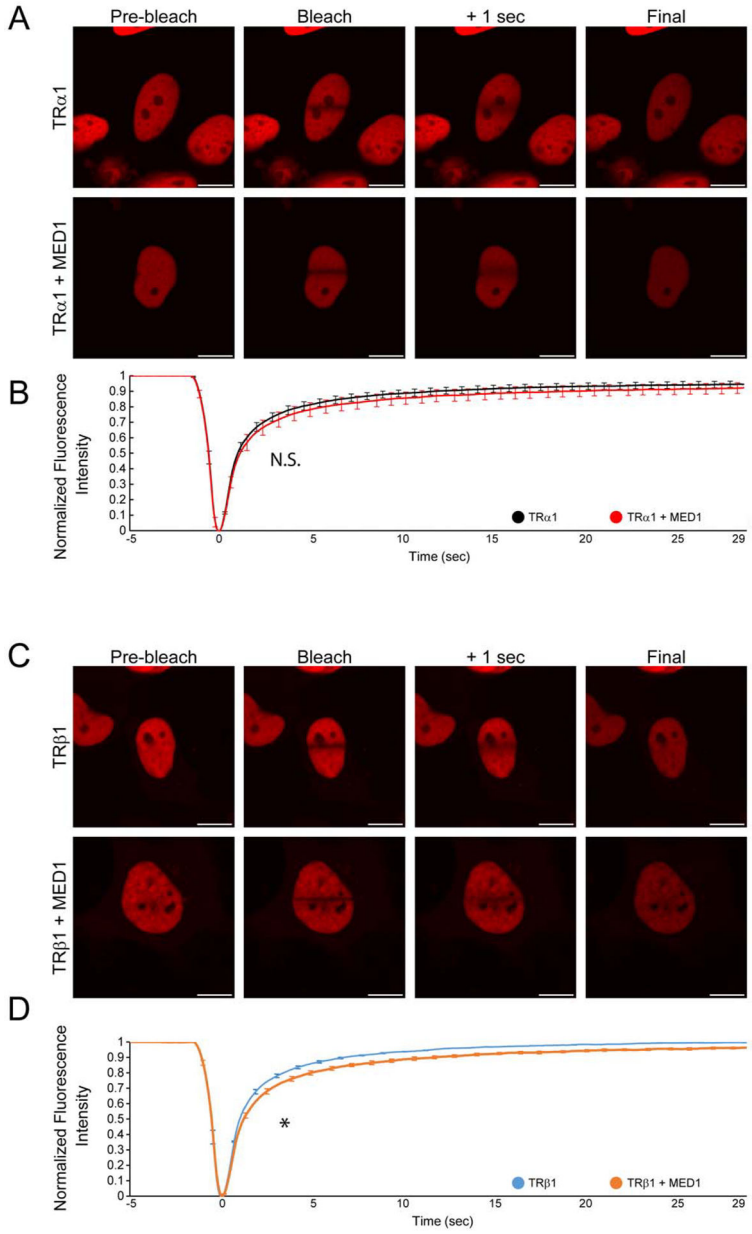

FIGURE 4.

MED1 differentially affects the intranuclear mobility of TR subtypes (A) HeLa cells were transfected with either mCherry-TRα1 expression plasmid or cotransfected with mCherry-TRα1 and GFP-MED1 expression plasmids, as indicated. Strip-FRAP was conducted on nuclei using a stimulation bleaching line near the midline of the nuclei. Representative images are shown for a nucleus prior to bleach (Pre-bleach), directly after bleaching was terminated (Bleach), 1 second post-bleach (+1 sec), and at the end of the recovery period (Final). Scale bar, 10μm. (B) FRAP curves compare normalized fluorescence intensity over time for TRα1 alone and TRα1 cotransfected with MED1. Error bars indicate ±SEM. Cotransfection of TRα1 with MED1 does not alter the intranuclear mobility of TRα1 (N.S., p>0.05; n=3 biological replicates, 20 nuclei per replicate). (C) HeLa cells were transfected

with either mCherry-TRβ1 expression plasmids or cotransfected with mCherry-TRβ1 and GFP-MED1 expression plasmids, as indicated and Strip-FRAP was conducted as described in (A). (D) FRAP curves from (C). Cotransfection of TRβ1 with MED1 reduces the halftime and mobile fraction of nuclear TRβ1 (*, $p<0.05$). Statistical analysis of intranuclear FRAP profiles is summarized in Table 1.

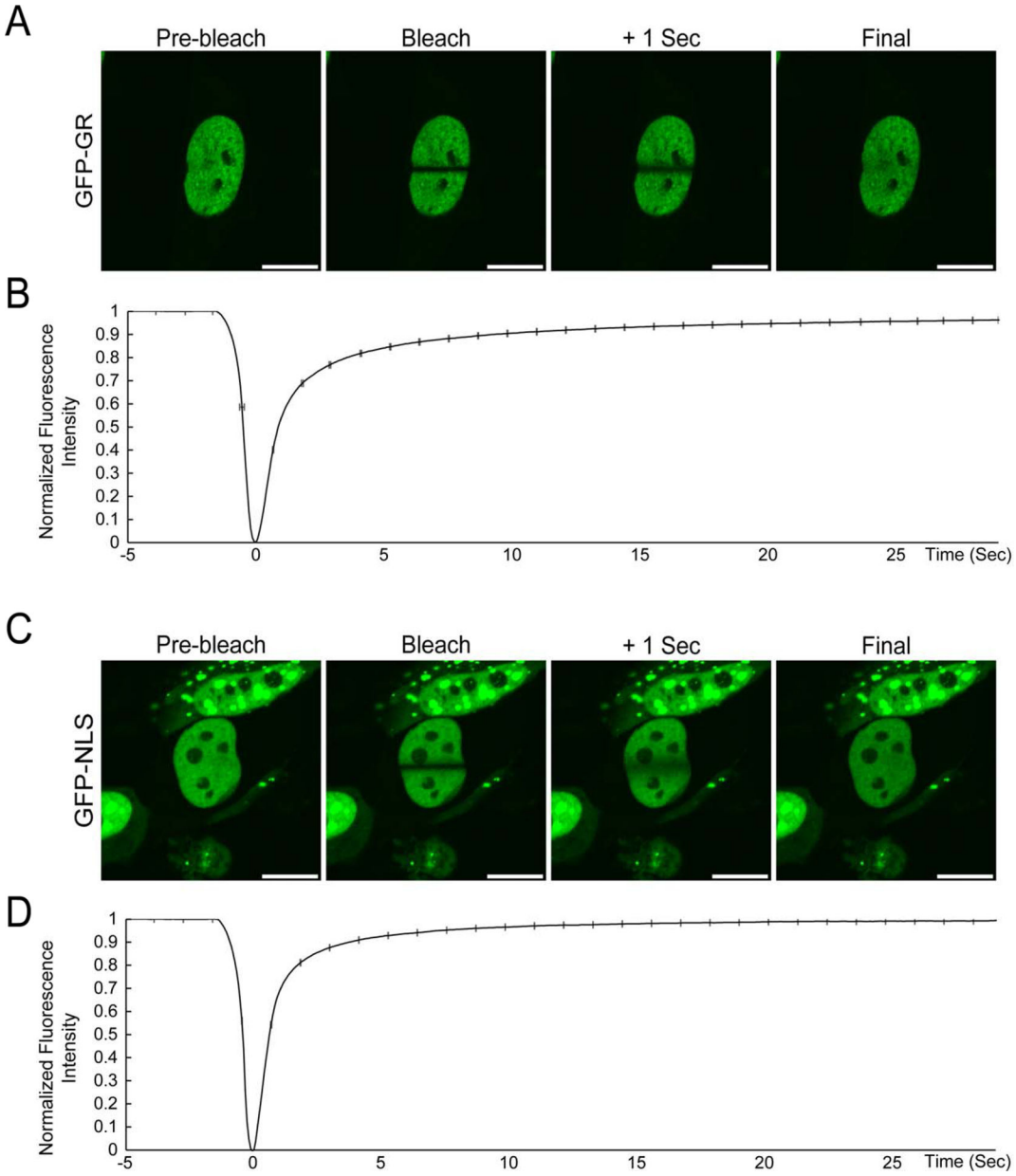

FIGURE 5.

Intranuclear dynamics of GFP-GR and GFP-GST-GFP-Hinge. (A) HeLa cells were transfected with GFP-GR expression plasmids and analyzed by strip-FRAP as described in Fig. 4. Of two mobility states for GFP-GR (fast, $t_{1/2}$=~0.6 sec; slow, $t_{1/2}$=~3.0 sec), the slower is displayed in the selected images. (B) FRAP curve depicting normalized fluorescence intensity over time for GFP-GR. Error bars indicate ±SEM. (n=3 biological replicates, 20 nuclei per replicate). (C) HeLa cells were transfected with an expression plasmid for GFP-GST-GFP-Hinge, a fluorescent fusion protein containing only the hinge domain of TRα1 with NLS-1 (see Fig. 1A). (D) FRAP curve for GFP-GST-GFP-Hinge. The fusion protein had a significantly faster rate of recovery than TR (see Fig. 4) (p<0.001).

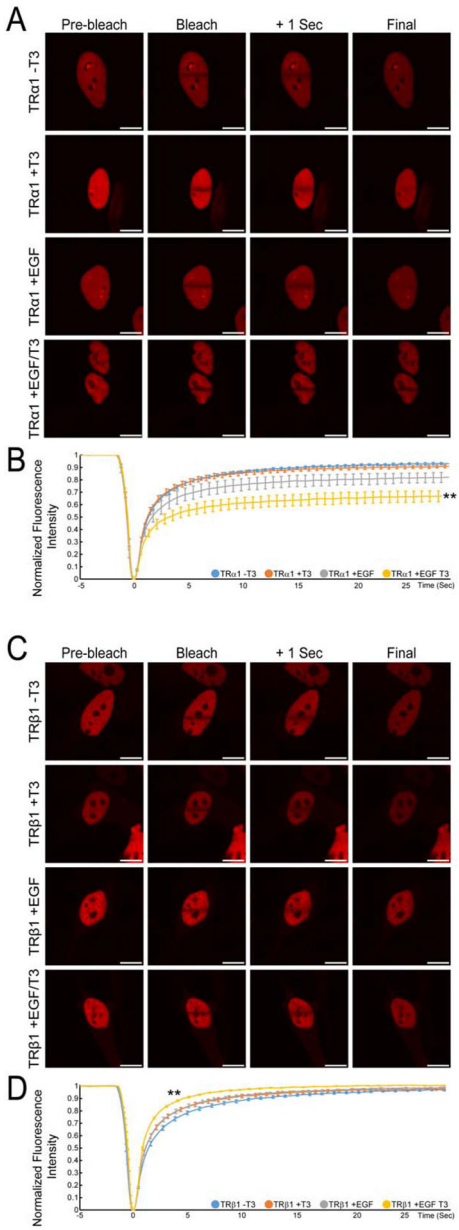

FIGURE 6.

Effect of T_3 and EGF on intranuclear mobility of TRα1 and TRβ1. (A) HeLa cells transfected with mCherry-TRα1 expression plasmids were incubated in charcoal-stripped FBS and T_3 (T3), EGF, or EGF and T_3, as indicated, and strip-FRAP was performed, as described in Fig. 4. Scale bar, 10μm. (B) FRAP curves compare normalized fluorescence intensity over time for TRα1 −T3 (blue), +T3 (red), +EGF (gray), and +EGF/T3 (orange). Error bars indicate ±SEM. EGF-treatment reduces the mobile fraction of TRα1, and EGF/T_3-treatment significantly alters the recovery rate, mobile fraction, and half-time slope (**, p<0.01; n=3 biological replicates, 20 nuclei per replicate). Statistical analysis of the intranuclear FRAP profiles is summarized in Table 1. (C) HeLa cells transfected with mCherry-TRβ1 expression plasmids were treated with T_3 (T3), EGF, or EGF and T_3, as

indicated and strip-FRAP was performed. (D) T_3 treatment significantly alters the recovery rate of TRβ1 ($p<0.05$), and EGF/T_3-treatment significantly alters the recovery rate, mobile fraction, half-time slope, and half-time of TRβ1 (**, $p<0.01$). Statistical analysis of the intranuclear FRAP profiles is summarized in Table 1.

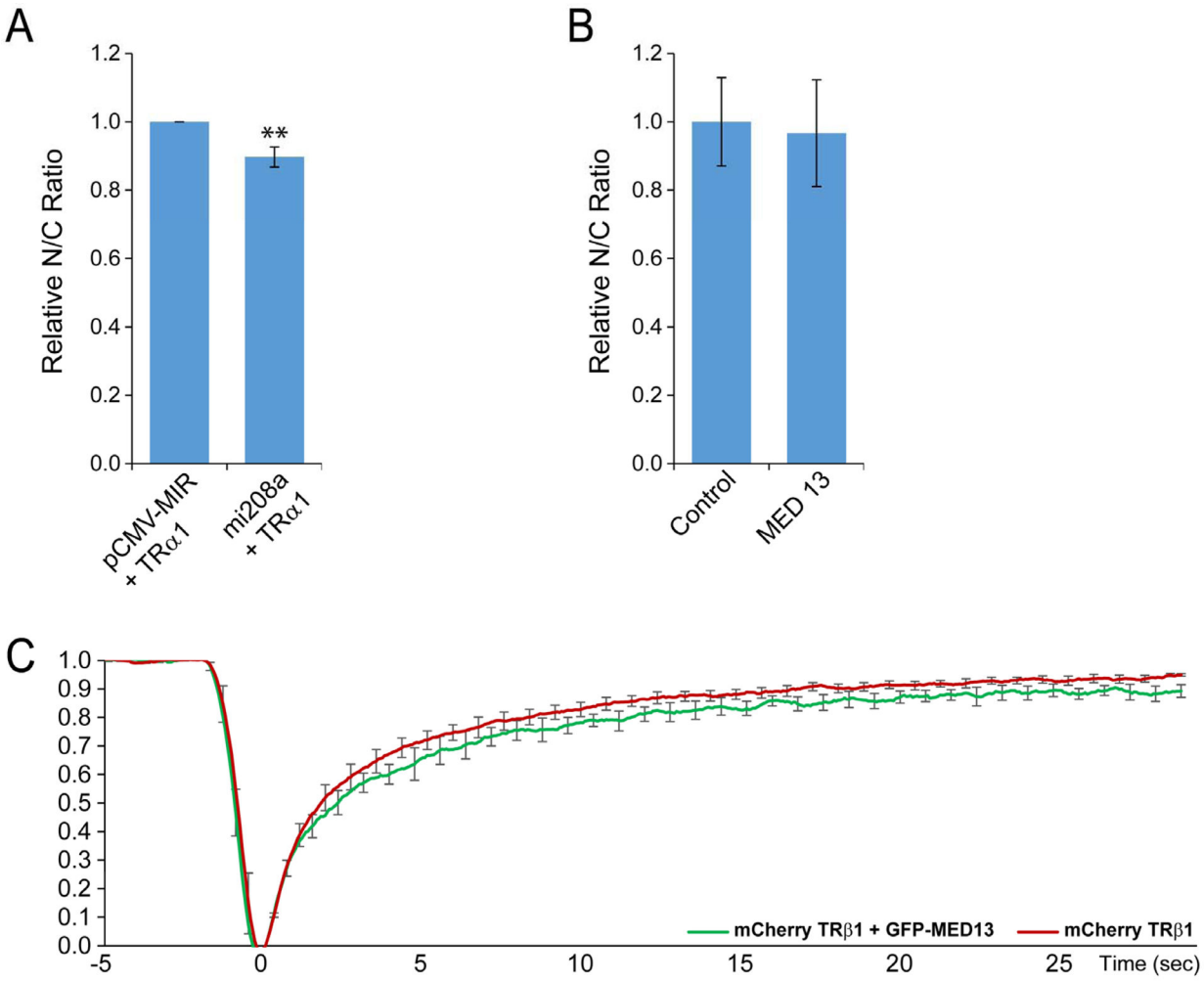

FIGURE 7.

Overexpression of miR-208a decreases TR nuclear retention. (A) HeLa cells were cotransfected with mCherry-TRα1 expression plasmid, and either pCMV-MIR, a scrambled miRNA and GFP expression plasmid, or with a combined miR-208a and GFP expression plasmid. Cotransfection was confirmed by visualization of GFP and mCherry fluorescence. Bars indicate the relative N/C ratio for TRα1 (average N/C ratio in miR-208a transfected cells normalized to the N/C ratio in pCMV-MIR-transfected cells). Error bars indicate ±SEM. Overexpression of miR-208a, which downregulates MED13, resulted in a significant increase in the cytoplasmic localization of TRα1, compared to overexpression of a scrambled, control miRNA (N/C<1.0; p=0.005636; n=4 separate, biologically independent replicates, 50–100 cells per replicate). (B) Overexpression of MED13 does not alter the nucleocytoplasmic distribution of TRβ1. HeLa cells transfected with mCherry-TRβ1 expression plasmid or cotransfected with mCherry-TRβ1 and GFP-MED13 expression plasmids, as indicated, were analyzed by fluorescence microscopy. Bars indicate the relative N/C ratio for TRβ1 (average N/C ratio in cotransfected cells normalized to the N/C ratio in single-transfected cells). Error bars indicate ±SEM. Cotransfection with MED13 yielded no change in intracellular distribution of TRβ1, compared with TRβ1 alone (N/C=1.0; N.S.,

p>0.05; n=3 biologically independent replicates; 100 cells per replicate). (C) HeLa cells were cotransfected either with mCherry-TRβ1 expression plasmids alone or cotransfected with GFP-MED1 expression plasmids, as indicated and strip-FRAP was performed. Overexpression of MED13 did not alter TRβ1's intranuclear FRAP profile (N.S., p>0.05; n=3 biologically independent replicates, 20 nuclei per replicate).

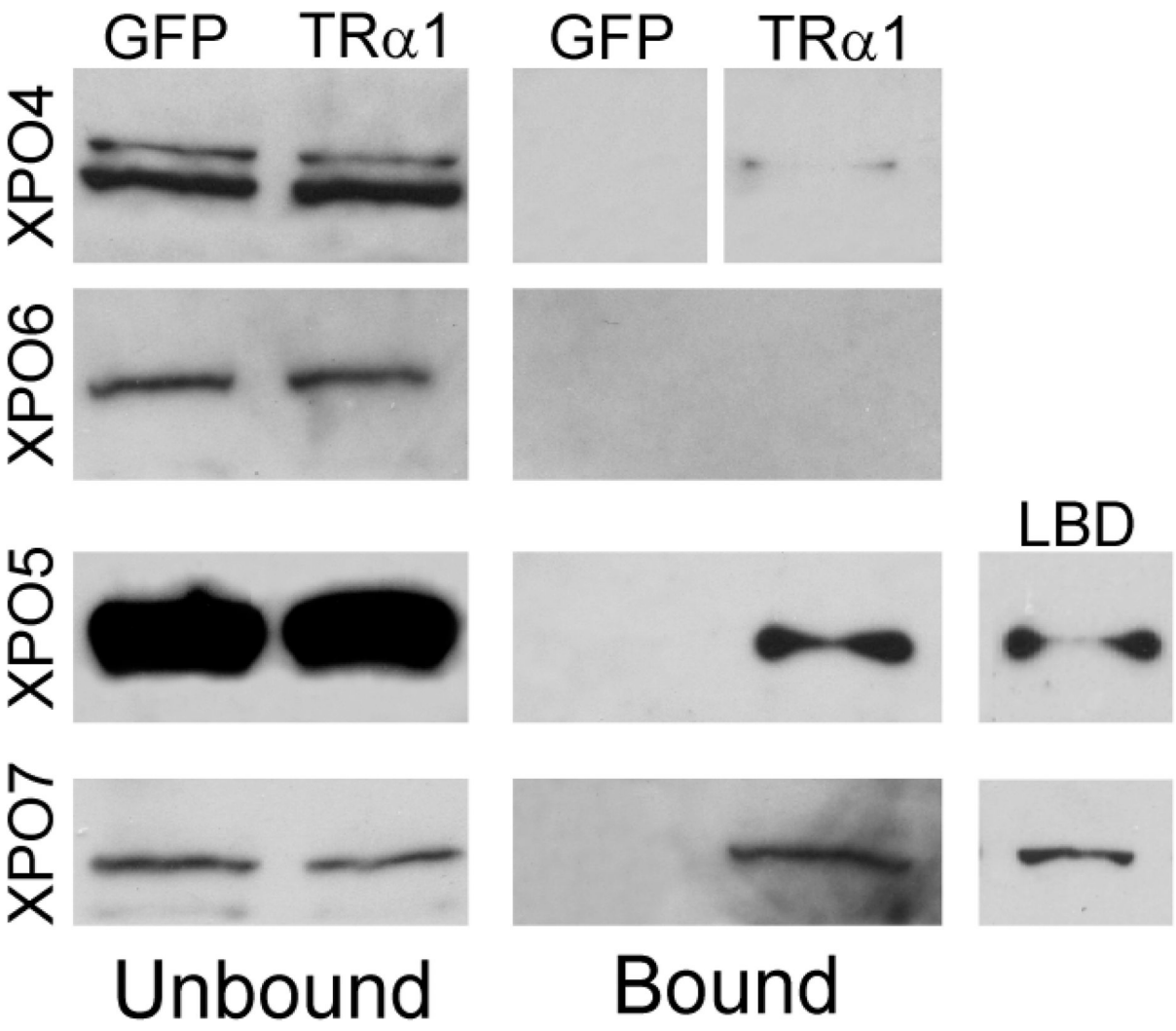

FIGURE 8.

Exportins 4, 5, and 7 coimmunoprecipitate with TRα1. HeLa cells were transfected with expression plasmids encoding GFP (27 kDa), GFP-TRα1 (73 kDa), or GFP-GST-GFP (G3)-Hinge-LBD (fusion protein containing the hinge region and ligand-binding domain of TRα1 (104 kDa), as indicated. Cell lysates were subjected to coimmunoprecipitation using immobilized anti-GFP-antibodies (GFP-Trap®_A). Representative immunoblots are shown (n=3–5 independent, biologically separate replicate experiments). Protein size was verified using Pre-Stained Kaleidoscope Protein Standards. Immunosupernatants (Unbound) and immunoprecipitates (Bound) from GFP, GFP-TRα1, and G3-Hinge-LBD-expressing cell lysates were analyzed on separate immunoblots, using longer exposure times for the immunoprecipitates, with exportin-specific antibodies to detect exportin 4 (127 kDa), exportin 5 (136 kDa), exportin 6 (129 kDa), and exportin 7 (110 kDa), as indicated.

Table 1.

Intranuclear FRAP profile for TRα1 and TRβ1

Treatment	Recovery Rate	Mobile Fraction	Immobile Fraction	Half-time Slope	$t_{1/2}$ (sec)
TRα1 (control)	0.011±0.000	0.946±0.034	0.054±0.034	0.552±0.090	1.009±0.177
TRα1 + MED1	0.011±0.001	0.922±0.053	0.078±0.053	0.493±0.161	1.211±0.420
	p=0.867	*p*=0.551	*p*=0.551	*p*=0.608	*p*=0.485
TRα1 -T3 (control)	0.013±0.001	0.932±0.017	0.068±0.017	0.441±0.074	1.256±0.194
TRα1 +T3	0.011±0.001	0.910±0.019	0.090±0.019	0.479±0.096	1.166±0.206
	p=0.222	*p*=0.208	*p*=0.208	*p*=0.612	*p*=0.612
TRα1 +EGF	0.011±0.001	0.822±0.068	0.178±0.068	0.340±0.171	1.795±0.916
	p=0.122	***p*=0.054**	***p*=0.054**	*p*=0.401	*p*=0.376
TRα1 +T3/+EGF	0.009±0.001	0.670±0.078	0.330±0.78	0.155±0.110	3.812±2.143
	***p*=0.020**	***p*=0.005**	***p*=0.005**	***p*=0.020**	*p*=0.109
TRβ1 (control)	0.012±0.001	0.999±0.003	0.001±0.003	0.596±0.045	0.920±0.078
TRβ1 + MED1	0.013±0.000	0.968±0.010	0.032±0.010	0.485±0.054	1.202±0.134
	p=0.156	***p*=0.007**	***p*=0.007**	***p*=0.053**	***p*=0.035**
TRβ1 -T3 (control)	0.014±0.001	0.970±0.011	0.030±0.011	0.397±0.055	1.368±0.169
TRβ1 +T3	0.013±0.000	0.976±0.020	0.023±0.020	0.508±0.071	1.099±0.169
	***p*=0.030**	*p*=0.653	*p*=0.653	*p*=0.099	*p*=0.124
TRβ1 +EGF	0.013±0.001	0.988±0.008	0.012±0.001	0.511±0.059	1.077±0.116
	p=0.092	*p*=0.089	*p*=0.089	*p*=0.070	*p*=0.070
TRβ1 +T3/+EGF	0.010±0.000	0.998±0.002	0.002±0.002	0.660±0.019	0.819±0.019
	***p*=0.002**	***p*=0.013**	***p*=0.013**	***p*=0.001**	***p*=0.005**